EPJ Web of Conferences **94**, 01056 (2015)
DOI: 10.1051/epjconf/20159401056

Explosive fragmentations of alumina (Al_2O_3) under quasistatic compressive loading

Qingyan Zhang[1], Xiaoqing Jin[1], and Fenghua Zhou[1,2,a]

[1] MOE Key Laboratory of Impact and Safety Engineering, Ningbo University, Ningbo 315211, Zhejiang, China
[2] The Faculty of Mechanical Engineering and Mechanics, Ningbo University, Ningbo 315211, Zhejiang, China

Abstract. Quasistatic compression tests for alumina (Al2O3) cylinders were conducted for the investigations of the compressive strengths and the dynamic fragmentation properties of the material. We focused on the post-failure dynamic fragmentation phenomenon. Most of the fragments were collected after tests, the shapes and sizes of these fragments were measured and statistically analyzed. The fragments were divided into three types on basis of their shapes and sizes, namely: the flaky medium sized fragments, the tiny debris, and the remaining large blocks, each type of the fragments were formed at different stages of the compressive failure-fragmentation process. The tiny debris were mainly generated from the "explosion" of the cylindrical specimen, in this stage the stored elastic energy within the specimen was released rapidly. The tiny fragments accounted the most part of the fragments in numbers. The average fragment size calculated by the proposed formula agree well with the experimental data.

1. Introduction

Due to their excellent mechanical properties of high hardness, high modulus and strength, low density, and good heat resistance, modern ceramics find broad applications in the area of protective engineering. Nevertheless, the materials are essentially brittle: having little fracture toughness and containing strength-limiting internal defects; Moreover, the tensile and compressive behaviors of the materials are asymmetric, with the compressive strength typically one order of magnitude higher than the tensile strength. The tension-compression asymmetry, in combinations with the material's brittleness, make ceramics easy to break into many pieces under different loading conditions. It is well known that under impact loading, the failure of a ceramic material is accompanied by a fragmentation process, when the material breaks (fragmentizes) into pieces millimeter or less in sizes [1–3]. Recent studies show that the compressive fragmentation are not limited to the impact loading cases. Under quasi-static compressive loading a ceramic specimen also fail in an "explosive" way [4,5].

The compressive fragmentation phenomenon can be understood from the energy point of view. Ceramics are strong to compression, with the compressive strength at the gigapascal (GPa) level. This means that at the failure point, the strain energy storage of the specimen is $1 \sim 10\,\mathrm{MJ/m^3}$. On the other hand, the high elastic modulus ($\sim$370 GPa) and the relatively low density ($4000\,\mathrm{kg/m^3}$) result in a very high fast crack speed (> 5000 m/s). Once failure starts, many cracks initiate and propagate within the specimen in a flash of time, fragmentizing the specimen and opening a way for the strain energy to release. This energy release process may occur in a time scale of $10^0 \sim 10^2 \mu$s order, making the failure more like an "explosive".

Understanding the failure behavior of the ceramics under quasi-static or impact loadings are crucial to the design and performance evaluation of a protective structure. One important issue in this study is to understand the dynamic fragmentation and the energy release process of ceramics under compressive loading. In the previous study [5], we experimentally investigated the compressive failure and fragmentation of brittle alumina under quasistatic compression. High speed videos showed that the failure of the specimen started with specimen splitting, and ended with dynamic fragmentations. An energy based fragmentation model was proposed to calculate the average post-failure fragment size.

In this paper, we extend the previous research, focusing on the post-failure dynamic fragmentation phenomena. The experimental set-up was improved so that most of the fragments can be recovered during a test. After each test, the sizes of these fragments were measured and statistically analyzed. Different types of fragments were found to be related to the different stages of compressive fragmentation. Theoretical model was used for the estimation of the average fragment size.

2. Quasistatic compression test

2.1. Specimen and test arrangement

Three kind of Al_2O_3 cylindrical specimens were made by hot-sintering 99.5% purity alumina powder. The dimensions of the specimen were 10mm diameter (Φ10) by 10 mm height, 10 by 20, and 20 by 40. The error of the upper and lower surfaces parallelism was less than 5 μm. Quasi-static compressive tests were conducted

[a] Corresponding author: zhoufenghua@nbu.edu.cn

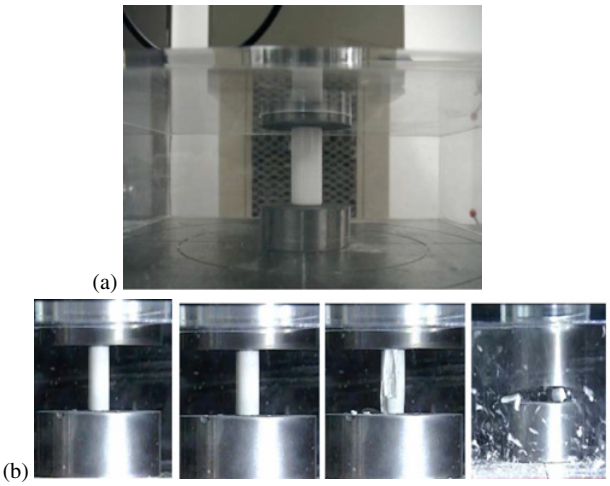

Figure 1. Quasi-static compression tests of Al_2O_3 cylinders: (a) the specimen and the WC anvils; (b) typical failure process.

on a servo-controlled hydraulic test machine with the maximum loading capacity 2000 KN. Tungsten carbide (WC) anvils were used between the specimen and loading platens to avoid indentations. Lubricant was applied on the interfaces between the anvils and the specimen to reduce friction. During the test process a high-definition video camera and a high-speed video camera were used to record the specimen failure process. The high speed video camera was triggered manually with 1 second pre-trigger time. To ensure that most fragments will be collected for further analysis, a rectangular cover made of transparent plexiglass was used to encapsulate the specimen, the WC anvils, and part of the loading platens, as shown in Fig. 1(a).

Quasi-static compression tests were conducted at an equivalent strainrate of 10^{-4} 1/s. The loading-strain curves show that the compressive deformation of the specimen is dominantly linear, with no observable signs of damage nucleation within the specimen. The compressive failure of the specimen occur as a sudden event, with immediate drop of loading stress, and always accompanied by explosive fragmentation. Figure 1(b) show a typical compressive failure/fragmentation process. The complete deform and failure process of a specimen include the stages of: 1) uniform deforming without observable damage initiation; 2) chipping when small debris fly out of the specimen surface; and sudden explosive failure.

2.2. Strength and fragmentation process

A total of 14 tests were conducted on different types of specimen. Table 1 collects the strengths of these specimen. Specimen with polished surface are apparently stronger than those unfinished. Most finished cylindrical specimen have strengths above 1GPa, except one specimen ($\Phi 20 \times 40$, No. 6) which had an observable surface damage near corner, and exhibited significantly low strength (0.22GPa). The strength scatters is shown in Fig. 2. Excluding the anomaly, smaller specimen tend to have higher strength than the larger ones

The failure of cylindrical specimens always accompany with fragmentations. The process when a specimen

Table 1. Strengths of Al_2O_3 cylinder specimen (GPa).

Specimen \ Test Number		1	2	3	4	5	6 (*)
Φ20×40	Polished	1.38	1.03	1.08	1.33	1.01	0.22
Φ10×20	Polished	1.58	0.8	1.14	-	-	-
	Unpolished	0.83	0.9	0.86	-	-	-
Φ10×10	Polished	1.71	1.03	-	-	-	-

* There existed an apparent surface damage area in this specimen.

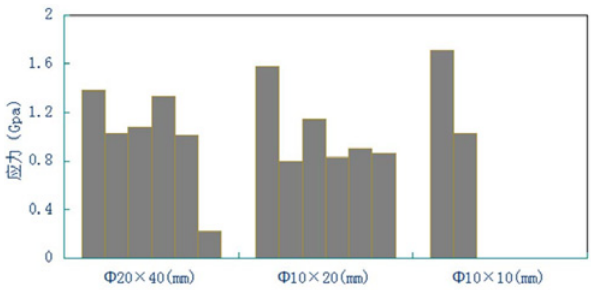

Figure 2. Scatters of compression strength.

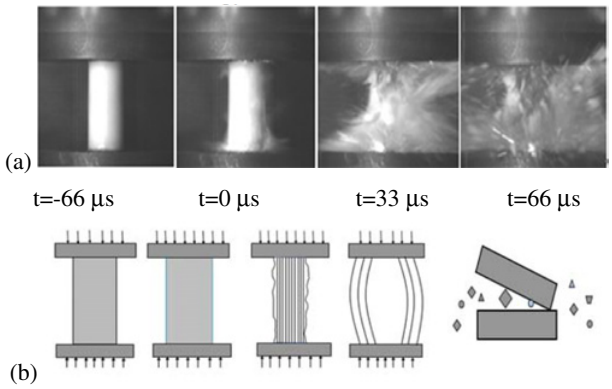

Figure 3. (a) High speed videos showing fragmentation process; (b) a schematic diagrams.

experience "explosive" fragmentation is shown in details by high speed videos in Fig. 3(a), and schematically explained in Fig. 3(b). In this process, the material fail at first with axial splitting, when many longitudinal cracks occur inside the specimen, splitting it into many columns. Under very large compression, the columns buckled and break into small pieces to release the stored strain energy.

The explosive fragmentation process were identical in all tests, whether the specimen was large or small. Typical fragmentation process occur within several dozens of μs. Always the bursting of specimen gave out a loud explosion sound and flashing light. There were discussions about whether the strain energy stored within the test machine would contribute to the fragmentation process. It appears that this energy flux is unlikely to happen. As Fig. 4(a) shows, once the failure occurs, the sudden loss of specimen loading capacity created an unloading wave in the elastic structures. This unloading wave would reflect at the specimen/anvil/platen interfaces as a tensile stress if they keep in contact, or cause separation if the interface

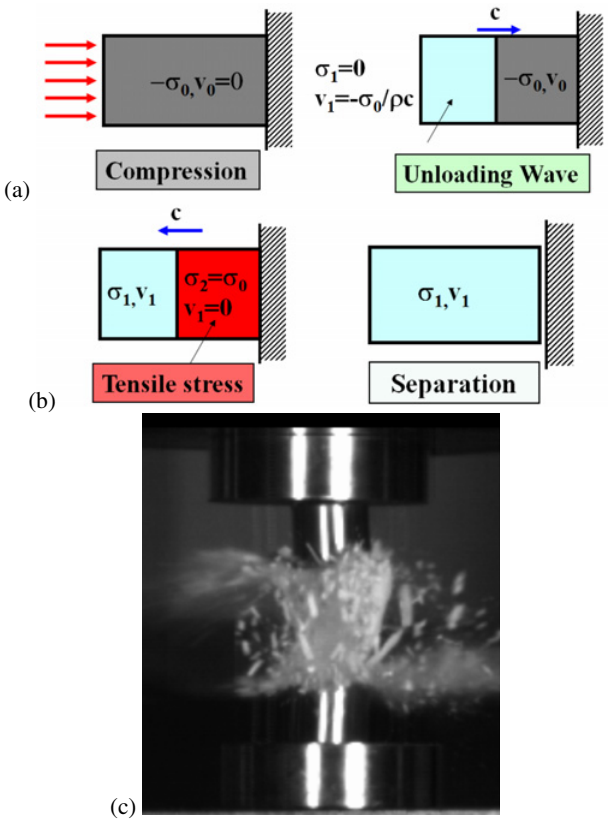

Figure 4. (a) Unloading waves propagation in elastic parts; (b) The reflections of the unloading wave on the interface, causing tensile stress of separations; (c) Separations of specimen-WC anvils.

cannot sustain tensile force (Fig. 4(b)). Eventually the specimen-anvil-loading platens interfaces separate, cutting off the energy flow from outside (Fig. 4(c)).

3. Fragment analysis

3.1. Fragment statistics

In each test, the fragments were contained in the plexiglass box and carefully collected. By comparing the total weight of the collected debris with the specimen weight, it can be concluded that most of the fragments were recovered. For each specimen, the debris statistical characteristics are similar, reflecting the fragmentation and energy release process. In this paper, we chose the three tests, each exhibiting the maximum compressive strength of same geometrical specimen group, namely, Sample **A** for the $\Phi 20 \times 40$ group specimen with compressive strength of 1.38GPa, Sample **B** for the $\Phi 10 \times 20$ group specimen with compressive strength of 1.58 GPa, and Sample **C** for the $\Phi 10 \times 10$ group specimen with compressive strength of 1.71 GPa.

For each sample, the sizes of the collected debris vary significantly. In current study we uses the debris size characterization method similar to that used for sediment grain size analysis in hydrological study [7]. Firstly different sieves were used to screen the fragments larger than 1.18 mm, and create the mass distributions of these "large" fragments. For the particles smaller than

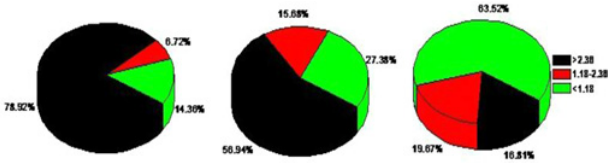

Figure 5. Mass distribution of large, medium, and small fragments in different samples: Sample A ($\Phi 20 \times 40$), B ($\Phi 10 \times 20$), and C ($\Phi 10 \times 10$).

1.18 mm size, a micro laser particle size analyzer was used to produce detailed quantitative statistical data.

In Fig. 5, the mass percentages of the large (sizes $>$ 2.36 mm), medium (sizes between 1.18 mm and 2.36 mm), and small (sizes $<$ 1.18 mm) fragments are shown for different samples. It is seen that the large/medium/small fragments ration are different for different types of specimen. For big specimen (Sample A), the large fragments ($>$ 2.36 mm) account for the major part of the total mass ($\sim$79%), while for small specimen (Sample C) the major mass part were the small fragments ($<$ 1.18 mm, mass ratio $\sim$64%). This phenomenon can be explained as following: On one side, the small specimen (Sample C, failed at 1.71 GPa) had less internal imperfections and failure at higher compressive stress, so that its dynamic crushing process was more "explosive", producing large quantities of small pieces. On the other side, the large specimen (Sample A) failed at relatively lower stress (1.38 GPa) resulting in larger fragments. Besides, after fragmentation some large chunks may remain at the specimen inner parts, accounting for the major mass percentage.

3.2. Fragment categorizations

The compressive fragmentation of a ceramic cylinder is a quite complex process, with different stages resulting fragments of different shapes and sizes. As Fig. 6(a) illustrates, the failure of the specimen starts at surface peeling in which some flake-shape (size in one direction significant smaller the sizes in the other two directions). At the ultimate "explosion" process, the split ceramic columns buckle-fractured into small, cubical shaped (the sizes in three directions similar) fragments. Most tiny fragments were created in this stage. If the stored strain energy is not so high, after the specimen broke, some inner parts of the specimen may remain, results in large blocks of rectangular and cubic shapes. The larger blocks of the specimen remnants are easy to identify. The middle sized flake debris and cubical debris can be identified by their shapes. Figure 6(b) shows the medium sized fragments collected in Sample C.

3.3. Medium and small fragment size statistics

As discussed above, the large chunks of the fragments, being the remnants of the explosive fragmentations, were not directly related to the dynamic fragmentation process. The middle and small size fragments are statistically analyzed. For the small fragments $<$ 1.18 mm, a laser particle size analyzer was used to measure the equivalent size of fragments. Here the equivalent fragment size was

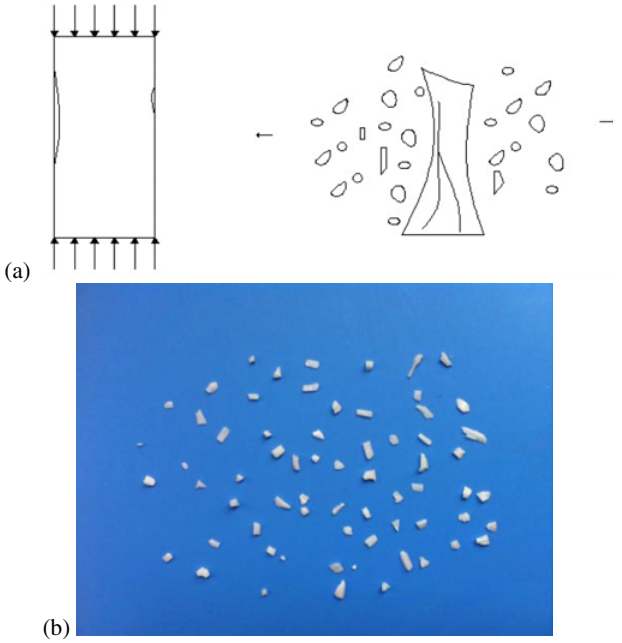

Figure 6. The different size fragments resulted from different fragmentation process: (a) surface fragment spallation; (b) fragmentation processes; c) The medium sized fragments (1.18 ∼ 2.36 mm) from sample C.

taken as the diameter of the sphere having the same volume of the fragment. Figure 7(a) gives the statistical distribution of the small fragments (< 1.18 mm) with their equivalent size. The fragments were in Sample B. It is seen that there exist two peaks for the small fragments, at 250 μm and 800 μm. Though detailed analysis of these distributions might be interesting, here we only focus on the average size of a total 3067 small fragments. Figure 7(b) shows the morphological appearances of some small fragments under scanning electron microscope. The geometrical shapes of these fragments were more or less like cubes or spheres, justifying the use of the equivalent size as the fragment measure.

For the group of medium size (1.18 ∼ 2.36 mm) fragments, the average fragment size were obtained by taking the picture of them (similar to Fig. 6(C)), then measuring the sizes using a image process software. Table 2 lists the average fragment sizes of all group, in each samples. The final average fragment size are taken as the number-weight average of the medium size group and the small size group.

4. Fragment size estimations

There exists many formulae for the estimations of fragment sizes [7–10]. We have proposed a model that linked the non-dimensional fragment size to the non-dimensional strain rate [11]:

$$\frac{s_{ave}}{s_0} = 4.5\left[1 + 4.5\left(\frac{\dot{\varepsilon}}{\dot{\varepsilon}_0}\right)^{2/3}\right]^{-1} \qquad (1)$$

where $s_0 = EG_c/\sigma_t^2$, $\dot{\varepsilon}_0 = c\sigma_t^3/E^2G_c$ are the characteristic fragment size and the characteristic strain rate of

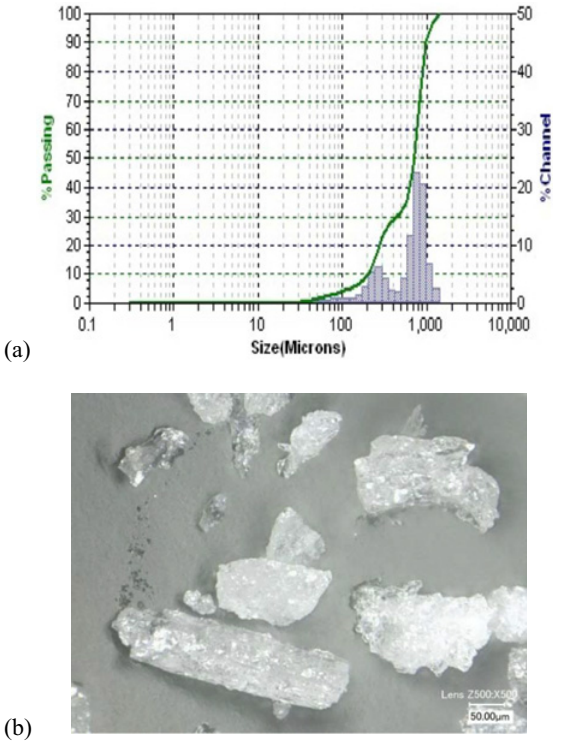

Figure 7. (a) Particle diameter analysis diagram of tiny debris (from Sample B, small size fragments); (b) Tiny fragments observed under SEM.

Table 2. Statistics of average fragments size.

Group \ Sample		A	B	C
1.18-2.36 (mm)	Mass (g)	3.295	0.954	0.660
	Numbers	320	96	63
	Ave. Size (mm)	1.7061	1.6985	1.7114
<1.18(mm)	Mass (g)	7.038	1.660	1.957
	Numbers	17696	3067	6335
	Ave. Size (mm)	0.5796	0.6437	0.5286
Experimental Average Size (mm)		**0.6000**	**0.6757**	**0.5402**
Theoretical Fragment Size (mm)		**1.31**	**0.922**	**0.63**

Table 3. Material parameters and characteristic quantities of Al_2O_3.

ρ g/cm^3	E GPa	c m/s	G_c N/m	σ_t MPa	$\dot{\varepsilon}_0$	s_0 mm
3.96	370	9700	40	150	5978	0.66

the material; E is the material's Young's modulus, G_c the fracture energy, σ_t the tensile strength, $c = \sqrt{E/\rho}$ the elastic wave velocity, and ρ the density. Table 2 listed the material data for the material. The s_0 and $\dot{\varepsilon}_0$ values thus calculated are 6000 s^{-1} and 0.66 mm, respectively.

It is notable that although the ceramic specimen was loaded quasi-statically, the sudden failure and fragmentation occur in a very short time and is undoubtedly dynamical. In the explosive fragmentation

Table 4. Estimation of fragments average size according to the theoretical formula.

Test	σ_c GPa	h mm	$\dot{\varepsilon}$ s^{-1}	$\dot{\varepsilon}/\dot{\varepsilon}_0$	s_{ave}/s_0	s_{ave} mm
A	1.36	40	*891.35*	0.1491	1.9860	*1.31*
B	1.58	20	*2071.08*	0.3464	1.3977	*0.92*
C	1.71	10	*4482.97*	0.97499	0.9546	*0.63*

process, the compressed columns of ceramic specimen buckle-bend rapidly, causing a tensile strainrate well above $10^3\ s^{-1}$. Following the method used in [5], The equivalent column expanding strainrate $\dot{\varepsilon}_0$ can be estimated by the energy balance theory: at the failure point the column has been pre-compressed to the compressive stress σ_c. Assuming that the total compressed energy has been transformed into the outward (radial) expanding kinetic energy, the expanding velocity of the fragmentizing part of the specimen is: $v = c\sigma_c/E$. Also assume that the column curvature radius is comparable to the specimen height h, the equivalent tensile strainrate is estimated by:

$$\dot{\varepsilon} = v/h = c\sigma_c/Eh. \tag{2}$$

Using the material parameters listed in Table 3, and the test conditions, the theoretical fragmentation parameters (equivalent tensile strainrate and average fragment size) can be estimated, as collected in Table 4.

The theoretically evaluated fragment sizes were also listed as the last row in Table 3 for comparisons. It is seen that experimental measured fragment size were generally smaller than, but pretty close to the theoretical estimations. This difference could be attributed to the experimental measurements that excluded the large fragment chunks without accounting for the stored strain energy in them. As the specimen size decrease, the theoretical estimations are closer to the experimental data, because the small specimen fragmentizes more significantly, namely, the small specimen (sample B and C) fragmentized completely. In whole, the theoretical model provided good fragment size estimations, better than simple order of magnitude. This model can be further extended to other ceramics and to the dynamical loading cases.

5. Summary

In this research we conducted quasi-static compression tests on three sizes Al_2O_3 cylinders. The compressive strength of the cylinders were measured. These strength show slight size dependence. The specimen explosively fragmentize after compression failure. The physics of these fragmentation phenomenon were explained from energy viewpoint. The fragments in each test were collected and analyzed. The fragments can be roughly classified into three types, each corresponding to different stage of the fragmentation process: the flaky medium sized fragments originated from surface spallation, the tiny debris generated from the "explosion" of the cylindrical specimen, and the large chunks remaining in the centre of the specimen. The tiny fragments accounted the most part of the fragments in numbers. The average fragment size calculated by using the standard formula agree reasonably well with the experimental measurement.

This research was supported by the National Science Foundation of China (NSFC) under Grants No 11272103, and by K.C. Wong Magna Fund of Ningbo University. The work has been presented in the 11th National Conference of Impact Dynamics in China.

References

[1] S. Sarva S. and S. Nemat-Nasser, Mat. Sci. Engng, **A317**(1-2): 140–144 (2001)
[2] W. Chen and G. Ravichandran, J. Mech. Phy. Solids, **45**(8): 1303–1328 (1997)
[3] H. Wang H. and K.T. Ramesh, Acta Materialia, **52**(2): 355–367 (2004)
[4] M.Y. Lee, R.M. Brannon and D.R. Bronowski, Sandia Report, SAND2004-6005 (2005)
[5] F. Zhou and Y. Wang, Proceeding DYMAT 2009: 1311–1316 (2009)
[6] Z. Niu and R. He, J. Sediment Res. 2002(5): 6–14 (in Chinese)
[7] D.E. Grady D.E., J. Appl. Phy. **53**: 322–325 (1982)
[8] L.A. Glenn and A. Chudnovsky, J. Appl. Phy. **59**: 1379–1380 (1986)
[9] W.J. Drugan, J. Mech. Phy. Solids, **49**: 1181–1208 (2001)
[10] V.B. Shenoy and K-S. Kim, J. Mech. Phy. Solids, **51**: 2023–2035 (2003)
[11] F. Zhou F., J-F. Molinari and K.T. Ramesh, Int. J. Frac. **139**:169–196 (2006)